Journal of Photochemistry and Photobiology A: Chemistry 204 (2009) 154–160

Contents lists available at ScienceDirect

Journal of Photochemistry and Photobiology A: Chemistry

journal homepage: www.elsevier.com/locate/jphotochem

Room-temperature fabrication of anatase TiO_2 submicrospheres with nanothornlike shell for photocatalytic degradation of methylene blue

Xiwang Zhang*, Jia Hong Pan, Alan Jianhong Du, Shiping Xu, Darren Delai Sun**

School of Civil and Environmental Engineering, Nanyang Technological University, 50 Nanyang Avenue, 639798 Singapore, Singapore

ARTICLE INFO

Article history:
Received 11 September 2008
Received in revised form 16 December 2008
Accepted 16 March 2009
Available online 24 March 2009

Keywords:
Titanium dioxide (TiO_2)
Submicrosphere
Rough shell
Photodegradation membrane filtration

ABSTRACT

A novel anatase TiO_2 submicrosphere with a rough shell of nanothorns was fabricated at room temperature by a chemical solution deposition technique using TiF_4. The resulting sample was characterized by field-emission scanning electron microscopy (FESEM), transmission electron microscopy (TEM), X-ray diffraction (XRD), nitrogen sorption measurements and Fourier transform infrared (FT-IR) spectrometry. The fabricated TiO_2 submicrospheres had a uniform size of about 500 nm. The shell of TiO_2 submicrospheres was covered by nanorods of 20–30 nm in diameter. These nanorods consisted of nanothorns which were 5–8 nm in diameter and about 20 nm in length. The unique rough shell resulted in higher absorbance because the light can have multiple reflections among nanorods and nanothorns. The TiO_2 submicrospheres exhibited similar performance as commercial nanoparticle TiO_2 (P25) on photocatalytic oxidation of methylene blue (MB). The TiO_2 submicrospheres were completely separated from treated water by membrane filtration without serious membrane fouling compared to P25. The durability test showed that the mechanical strength and photocatalytic activity are stable enough for multiple recycling. This environmentally friendly and energy efficient method may pave way for new photocatalyst design.

1. Introduction

Over the last three decades, semiconductor-mediated photocatalysis has been intensively investigated as a promising environmental purification technology [1–4]. Nanosized TiO_2 is the most widely used photocatalyst because of its higher activity than its bulk counterpart. However, there is a huge barrier on application of these nanosized TiO_2 materials. Due to their size, it is difficult to separate these nanosized photocatalysts from the treated water. In addition, nanosized TiO_2 aggregates easily, which leads to lower efficiency [5].

TiO_2 microspheres and submicrospheres have drawn increasing attention due to their ease of recovery under gravity or via membrane filtration [6–8]. Nagaoca et al. [9] reported carbon/TiO_2 microspheres prepared form cellulose/TiO_2 microsphere composites. Zhang et al. [10] prepared TiO_2 porous microspheres by reversed suspension polymerization and sol–gel method. Li et al. [6] fabricated TiO_2 microspheres with a diameter of 30–160 μm via a method of sol-spraying-calcination. Our group [11,12] fabricated TiO_2/Al_2O_3 microspheres with a particle size of 180–250 μm via similar method. Unfortunately, for all the mentioned microspheres, only the external surface has the chance of being irradiated by UV light which limits the photonic efficiency. Grime [13] and Wang [14] have proved that macroporous channel could serve as light-transfer path for the distribution of photon energy so that the internal surface of macroporous spheres can also be utilized. Okuyama's group [15] fabricated brookite TiO_2 spheres with macroporous structure by spray-drying a mixing suspension of brookite nanoparticles and polystyrene latex (PSL) particles. Wang et al. [16] prepared porous crystalline TiO_2 submicrospheres via controlled hydrolysis of titanium tetraisopropoxide. Li et al. [17] fabricated porous TiO_2 microspheres with tunable chamber structure via solvothermal method. Ho et al. [18] synthesized hierarchical porous TiO_2 microspheres via hydrothermal treatment. Our group [19,20] fabricated porous TiO_2 hollow aggregates with openings via a low-temperature hydrothermal method and macroporous basketry-like TiO_2 (B) microspheres consisted of nanowires via hydrothermal-spray-drying process, respectively. However, the mechanical strength of these porous spheres was not as strong as that of solid spheres. Most recently, some solid microspheres with rough shell have been reported. Yao et al. [21] have fabricated CdS and CdSe nanoflowers or nanotrees via a solvothermal approach. Gao et al. [22] reported high porous TiO_2 microspheres using a supersaturated aqueous solution containing peroxotitanium complex ions. These rough microspheres have higher external surface

* Corresponding author. Tel.: +65 6790 6914; fax: +65 6861 5254.
** Corresponding author. Tel.: +65 6790 6273; fax: +65 6791 0676.
E-mail addresses: XWZhang@ntu.edu.sg (X. Zhang), DDSun@ntu.edu.sg (D.D. Sun).

1010-6030/$ – see front matter © 2009 Elsevier B.V. All rights reserved.
doi:10.1016/j.jphotochem.2009.03.011

area than smooth microspheres, which results in higher UV–vis light absorbance.

Recently, fabrication of TiO_2 films and nanostructures with desired crystallographic phase via hydrolyzing titanium organic salts in aqueous solution at low reaction temperature has generated significant interest [23–27]. This liquid-phase deposition (LPD) is low-energy and environmentally friendly. In this paper, for the first time, a new type of TiO_2 submicrospheres with rough nanothornlike shell was fabricated at room-temperature by LPD method using aqueous solution of TiF_4. The advantages of the present products are as follows. (1) UV–vis light can be well utilized by having multi-reflections on the nanothorns resulting higher absorbance, enhancing photonic efficiency. (2) TiO_2 submicrospheres are easily reclaimed and reused by membrane filtration without serous membrane fouling owing to their relatively larger diameter.

2. Experimental

2.1. Synthesis of TiO_2 submicrospheres

TiF_4 (Aldrich) was dissolved in deionized water contained by plastic bottle to gain a 0.04 M solution. Aqueous ammonia ($NH_3{\cdot}H_2O$, 2.0 M) was added into the TiF_4 solution dropwise under vigorous stirring until the pH of the solution reach 2.6. The solution was put in capped plastic bottle and maintained at $25 \pm 2\,^{\circ}C$ for 24 h. After the reaction, the white products were collected and washed with deionized water. After air-dried at room temperature, the samples were kept in a vacuum vessel.

2.2. Characterization of TiO_2 submicrospheres

The morphologies of the TiO_2 submicrospheres were examined using a field-emission scanning electron microscope (FESEM, Jeol JSM-6340F, 5 kV) and a transmission electron microscope (TEM, JSM 2010, 200 kV). X-ray diffraction (XRD) patterns were obtained using Bruker (Germany) AXS D8 Advance (Cu Kα, λ = 1.5406 Å). The scanning rate was $0.02\,^{\circ}/s$ in 2θ mode from 20° to 80°. Nitrogen adsorption–desorption isotherms were obtained at liquid nitrogen temperature (77 K) using a Quantachrome Autosorb1 instrument. Before the measurement, the samples were outgassed under vacuum for 5 h at 150 °C. Fourier transform infrared (FT-IR) spectra on pellet of the sample mixed with KBr were recorded on a PerkinElmer spectrum GX FT-IR spectrometer at a resolution of 5 cm^{-1}. A Jasco V-550 UV–vis spectrophotometer equipped with an integrating sphere attachment (ISV-469) was used to obtain the reflectance spectrum of the TiO_2 submicrospheres over a wavelength range of 200–800 nm.

2.3. Photocatalytic activity measurement

The photocatalytic activity of the TiO_2 submicrospheres was investigated by photodegradation of methylene blue (MB) in aqueous solution. The UV light source, an 11 W Upland 3SC9 Pen-ray lamp (254 nm) was immersed into reactor containing 500 mL 20 mg/L MB solution. The dosage of the TiO_2 submicrospheres was 0.5 g/L. Dark absorption of MB on the TiO_2 submicrospheres was carried out for 30 min under air bubbling prior to photocatalytic reaction. Commercial P25 TiO_2 (Degussa, BET area, ca. 50 m^2/g; particle size, 20–30 nm) was also tested under identical conditions as a reference. Change of MB concentration in solution was measured by monitoring the absorbance at 666 nm on a UV–vis spectrophotometer (Shimadzu UV-1700, Japan) after diluted 1.5 times, and the total organic matter (TOC) concentration was measured on a Shimadzu TOC-Vcsh TOC analyzer. Before analysis, catalysts in the samples were removed by filter (0.20 μm).

2.4. Reclamation of used TiO_2 submicrospheres

Membrane filtration was conducted to separate and reclaim the used TiO_2 submicrospheres from the treated water. A dead-end membrane filtration cell (Millipore) was used with microfiltration membrane (ADVANTEC MFS Inc., 0.20 μm) under a transmembrane pressure of 0.75 MPa. The permeation flux of membrane was then calculated from the permeate collected as follows:

$$J = \frac{\Delta V}{A \cdot \Delta t} \tag{1}$$

where J is permeation flux (L/m^2 h), ΔV volume change of permeate (L), A area of membrane (m^2), Δt filtration time (h). The turbidity of solution before and after filtration was then recorded using a turbidimeter (Hach 2100N) to calculate the rejection rate of TiO_2 submicrospheres by membrane filtration. The resistance-in-series model was applied to evaluate the fouling characteristics of photocatalyst during filtration. According to this model, the permeation flux, J can be expressed as follows [28,29].

$$J = \frac{\Delta P}{\mu R_t} = \frac{\Delta P}{\mu(R_m + R_c + R_p)} \tag{2}$$

where ΔP is the transmembrane pressure (Pa), μ the viscosity of permeate (Pa s), R_t the total resistance (m^{-1}), R_m the intrinsic membrane resistance, R_c the cake resistance, and R_p the fouling resistance due to pore blockage. The experiment procedure to reach each resistance value was referred to previous study [30].

3. Results and discussion

3.1. Characterization of TiO_2 submicrospheres

Fig. 1 shows FESEM images of the TiO_2 submicrospheres at different magnifications. Submicrospheres were mass produced by the present room-temperature synthesis method. Fig. 1a and b shows that these microspheres have a uniform diameter of about 500 nm. Furthermore, the submicrospheres possess a unique rough shell, which composes of nanorods with 20–30 nm in diameter as observed from high magnification FESEM images (Fig. 1c and d). The nanostructure of the submicrospheres was also examined by high-resolution TEM. Fig. 2 shows a set of TEM images of the sample at different magnifications. The rough shell of these submicrospheres was further revealed by TEM micrographs. It can be found from Fig. 2b and c that the nanorods on the submirospheres consisted of smaller nanothorns. These nanothorns were of 5–8 nm in diameter and about 20 nm in length. A uniform fringe spacing of 3.52 Å was found on the nanothorns as shown in Fig. 2d, which is indexed to the (1 0 1) plane of the anatase TiO_2. It indicated that these nanothorns were grown to the surface of the submicrosphere along the (1 0 1) plane. It was presumed that the nanothorns were grown on some defect sites of the initial single-crystal nuclei [23].

A systematical investigation found that pH of TiF_4 solution and reaction temperature has huge influence on the structure of the TiO_2 submicrospheres. Fig. 3a and b shows the samples fabricated at different pH, 2.3 and 3.0, respectively. Uniform size of TiO_2 submicrospheres with nanothorn crystallites on their shell was gained. However, they are about 400 nm in diameter which was smaller than that of these fabricated at pH of 2.6. The output of submicrospheres was also lower than that at pH of 2.6. After increasing the pH to 3.0, the size of the products did not increase significantly. Instead their particle size becomes non-uniform, many small particles were found in the sample. TiO_2 was produced by the stepwise reaction in supersaturated TiF_4 solution at pH 1–3 as following [24,31,32].

$$TiF_4 \rightarrow\rightarrow Ti[OH]_{4-x}F_x \rightarrow\rightarrow TiO_2 \tag{3}$$

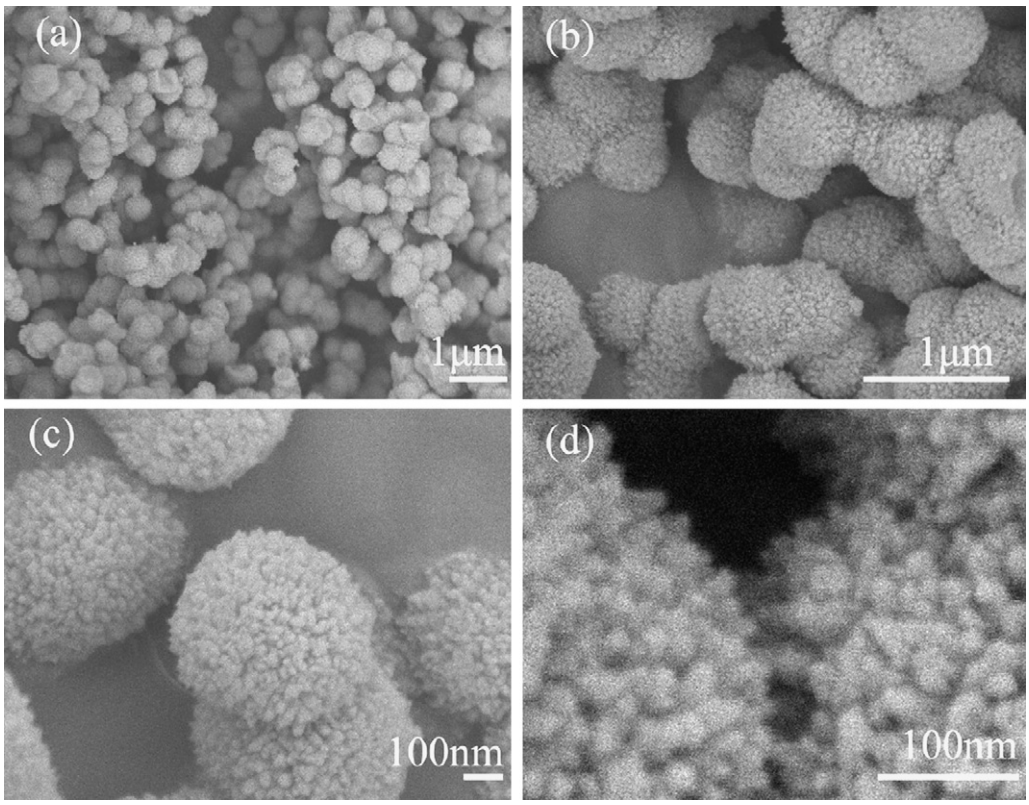

Fig. 1. (a–d) FESEM images of the TiO_2 submicrospheres at different magnifications.

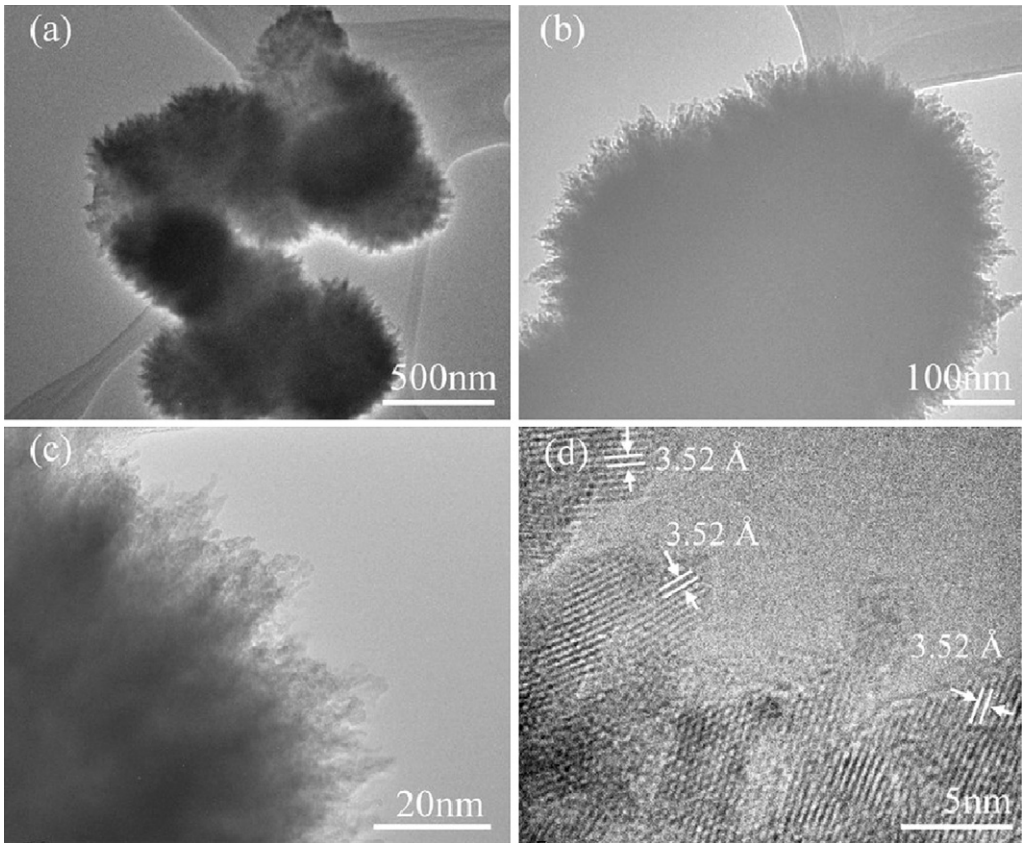

Fig. 2. (a–d) TEM images of the TiO_2 submicrospheres at different magnifications.

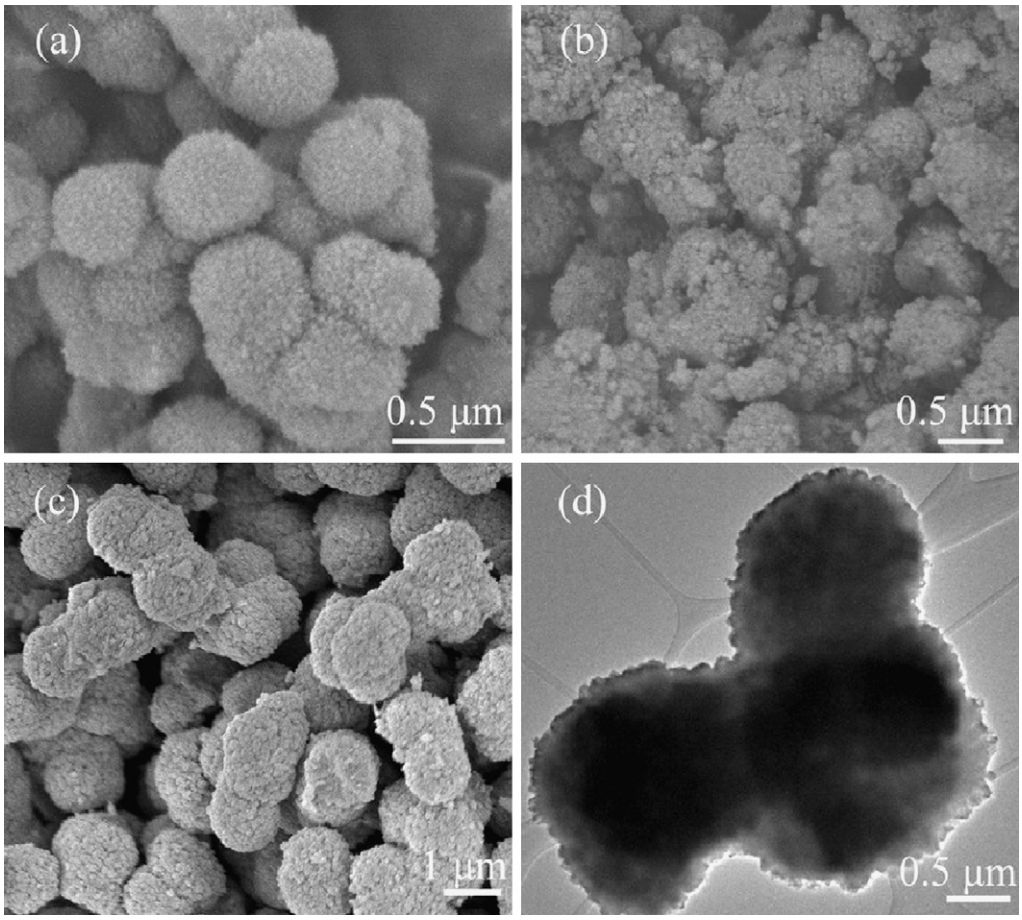

Fig. 3. (a) and (b) FESEM images of the TiO_2 submicrospheres fabricated at pH 2.3 and 3.0, respectively; (c) FESEM and (d) TEM image of the TiO_2 submicrospheres fabricated at 60 °C.

Yang et al. [23] has found that both heterogeneous nucleation and growth depended on pH condition. Heterogeneous nucleation and growth are retarded at low pH condition so that the TiO_2 spheres were small and the output was low. At higher pH heterogeneous nucleation and growth were dramatically promoted resulting that the TiO_2 submicrospheres become loose [23]. Nanothorns on the shell of the TiO_2 submicrospheres disappeared when the reaction temperature increased to 60 °C as shown in Fig. 3c and d. It indicated that higher reaction temperature inhibits the formation of nanothorns on the shell of submicrospheres.

The crystal phase and composition of the TiO_2 submicrospheres were also characterized by XRD. Fig. 4a shows the wide-angle XRD patterns of the samples. The XRD patterns of the samples match well with anatase TiO_2 (JCPDS 21-1272). No additional peaks of other impurities were detected. This result illustrated that the synthesized submicrospheres by this method were pure anatase TiO_2. The average crystal size of the sample has been estimated to be around 5 nm by using Scherrer's formula. The FTIR spectrum of the TiO_2 submicrospheres is shown in Fig. 4b. The absorbances between 500 and 900 cm^{-1} originate from TiO_2 [19]. Two bands at 3400 and 1650 cm^{-1} are related to the surface adsorbed water and hydroxyl group [33], which are crucial in photocatalytic reactions; they will react with photo-excited holes on the catalyst surface and produce hydroxyl radicals, which is the major oxidant in degrading organic pollutants. The surface area and porosity of the TiO_2 submicrospheres were confirmed using nitrogen sorption analysis. Fig. 5 shows the pore size and nitrogen adsorption and desorption isotherms for the sample. The BET surface area is 19.8 m^2/g. The pore size distribution plot shows that these submicrospheres have mesoporous structure and the mean pore diameter is 2.7 nm.

Fig. 6 shows the UV–vis absorbance spectra of the sample. Absorbance (A) is an indicator of light absorption ability, with higher A value representing stronger photoabsorption capability. As seen in Fig. 6, the TiO_2 submicrospheres exhibited strong capability of light absorption in the range of 200–400 nm, as indicated by the higher A value. This is not surprising because of the rough external shell. When a UV light illuminated onto a catalyst with smooth shell, some of light would be reflected. Compared to smooth shell, the rough shell with nanothorns of the submicrospheres can absorb more UV–vis light because the UV–vis light can have multiple-reflections among the nanothorns.

3.2. *Photocatalytic activity of TiO_2 submicrospheres*

Photocatalytic activity of the TiO_2 sumcriospheres was evaluated by photocatalytic degradation of MB in aqueous. Fig. 7 shows the variations of absorption spectrum of MB during photocatalytic oxidation by the TiO_2 submicrospheres. The absorbance peaks of 620 and 666 nm at visible region dramatically disappeared while the absorbance peaks of 250 nm and 292 nm at UV region declined with slower rate. The concentration changes of MB and TOC for various reaction times are shown in Fig. 8. It was found that the more MB adsorbed on P25 than on the submicrospheres, which was attributed to higher surface area of P25 than the latter. The photocatalytic degradation generally follows a Langmuir–Hinshelwood mechanism, which could be simplified as a pseudo-first order

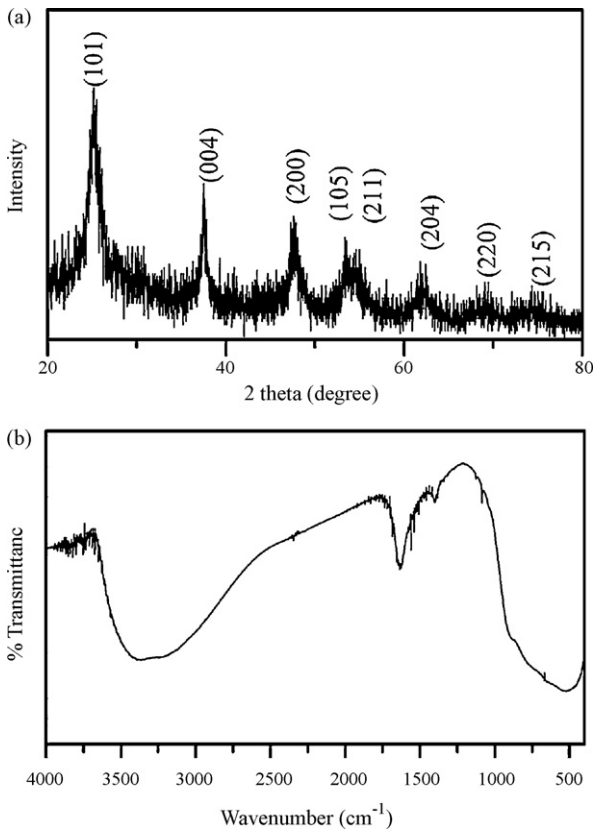

Fig. 4. (a) XRD pattern and (b) FT-IR spectrum of the TiO_2 submicrospheres.

reaction as follows [1,34].

$$r = -\frac{dC_t}{dt} = kC_t \quad (4)$$

where r is the degradation rate of reactant. C the concentration of reactant. k the apparent reaction rate constant. The photocatalytic degradation of MB by P25 and the TiO_2 submicrospheres followed first order kinetics. The k for the TiO_2 submicrospheres was $0.0515\,min^{-1}$ while $0.0542\,min^{-1}$ for P25. As mentioned above, the BET surface area of the TiO_2 submicrospheres ($19.8\,m^2/g$) is only two fifth of that of P25 ($50\,m^2/g$). The intrinsic potocatalytic activity defined using initial degradation rate per unit surface area

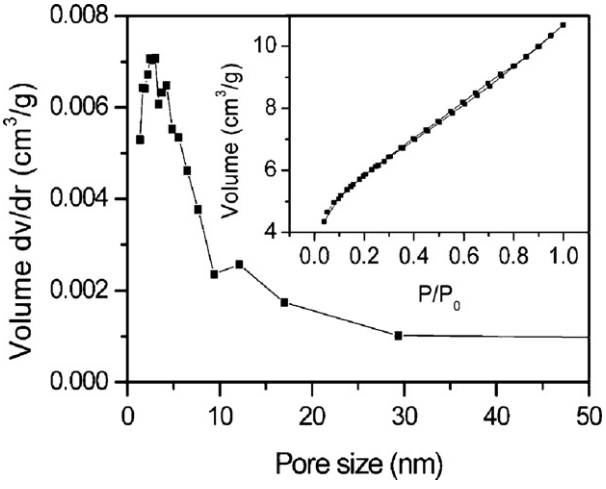

Fig. 5. BJH pore size distribution curve of the TiO_2 submicrospheres. The inset shows nitrogen adsorption–desorption isotherm.

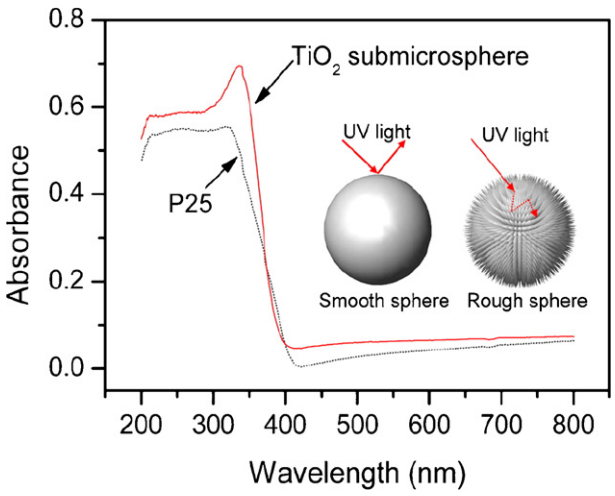

Fig. 6. UV–vis absorbance spectra of the TiO_2 submicrosphere and P25.

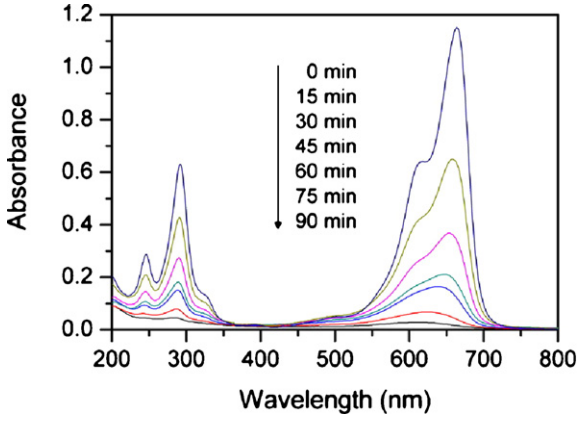

Fig. 7. Changes of absorption spectra of MB solution during photocatalytic degradation by TiO_2 submicrosphere (diluted 1.5 times).

[35] for TiO_2 submicrospheres is $8.29 \times 10^{-6}\,mol\,h^{-1}\,m^{-2}$. It is 2.4 times of that of P25 ($3.45 \times 10^{-6}\,mol\,h^{-1}\,m^{-2}$). It was surprising that the TiO_2 submicrospheres exhibited such activity. This may be explained by the following factors. On the one hand, the higher light absorption capability of the TiO_2 submicrospheres due to their rough shell contributes to the good photocatalytic activity; one the other hand, for the commercial nanosized P25, they usually do not present individually in aqueous system. These nanosized particles aggregated to up to 0.1 μm, which results in decrease of photocatalytic activity [36]. The TOC results followed similar trends with MB. However, the TOC removal rates were much slower than

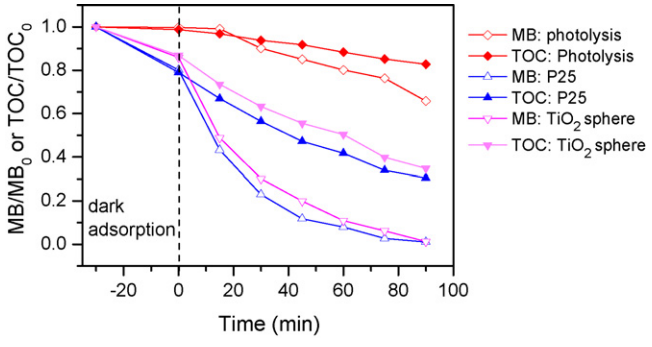

Fig. 8. Changes of MB concentration and TOC during photolysis and photocatalytic degradation in the presence of P25 and the TiO_2 submicrosphere.

these of MB. This is because that MB was first decomposed into small molecular matter prior to into carbon dioxide and water [37].

Membrane filtration was used to separate the TiO_2 submicrospheres after photocatalytic oxidation. The turbidity in the filtrate decreased nearly zero from about 900 NTU in the feed, which means that the TiO_2 submicrospheres were completely separated. In order to determine the effect of the presence of TiO_2 submicrospheres on membrane filtration performance, especially on membrane fouling, the membrane flux was measured during filtration and the result is shown in Fig. 9. P25 suspension was also filtered as a reference. As shown in Fig. 9, the membrane flux decreased dramatically at the beginning of filtration of both TiO_2 submicrospheres and P25 suspensions due to the formation of cake layer on membrane surface. After 30 min the membrane flux of TiO_2 submicrospheres became stable while a slow decline was also found for P25. After 200 min of filtration, the membrane flux of TiO_2 submicrospheres was 82.5 L/h m^2, which was 2.2 times that of P25 (37.1 L/h m^2). The resistances of membrane, cake layer and pore blockage were measured and the results are shown in Fig. 10. It was found that the resistance was mainly attributed to cake layer after 200 min of filtration. The resistance of TiO_2 submicrosphere cake layer was 30.5 m^{-1}, which was only 44% of that P25 (69.0 m^{-1}). The low resistance of TiO_2 submicrosphere cake contributed the large particle size of TiO_2 sumicrospheres. The cake layer was formed by catalyst depositing on membrane surface and its resistance depended on the size of gap between catalysts which was channel of water stream during filtration (inserted schematic diagram in Fig. 9). Larger size of TiO_2 submicrospheres results in larger gap between catalysts compared to P25, resulting in lower cake resistance. Moreover, pore blockage resistance of TiO_2 submicrospheres was much less than that of P25 as shown because the size of TiO_2 submicrosphere is larger than membrane pore size so that no TiO_2 submicrosphere can enter membrane pores.

To investigate stability of the rough TiO_2 submicrospheres on photocatalytic activity and mechanical strength, the same sample was repeatedly used for 10 times after separation via membrane filtration. The removal rates of MB and TOC in every cycle are shown in Fig. 11a. There were no dramatic decreases on the removal rate of

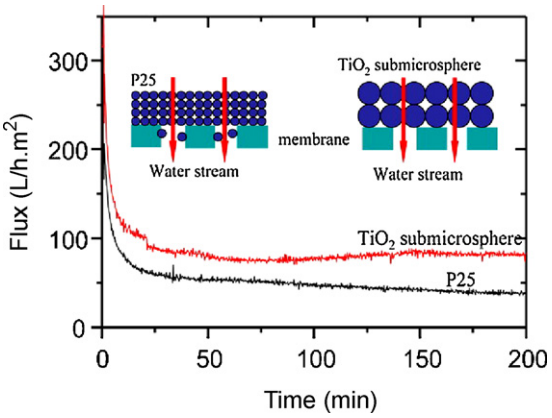

Fig. 9. Changes of membrane flux during filtration of TiO_2 submicrosphere and P25 suspensions after photocatalytic oxidation. Insert: Schematic diagram of membrane fouling caused by different size photocatalysts.

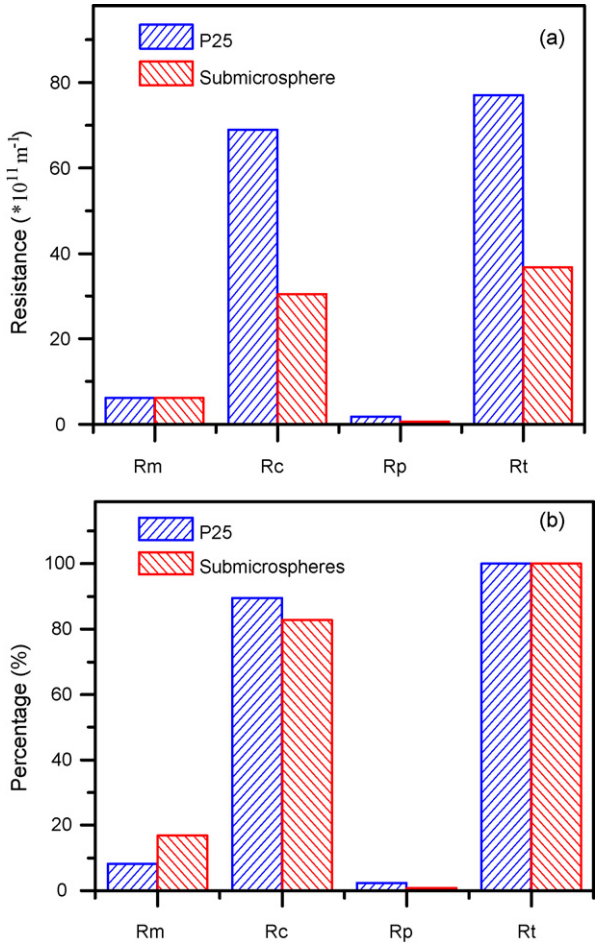

Fig. 10. Summaries of resistances for the MF filtration of P25 and TiO_2 submicrosphere suspensions. (a) Value and (b) the percentage over the total resistance.

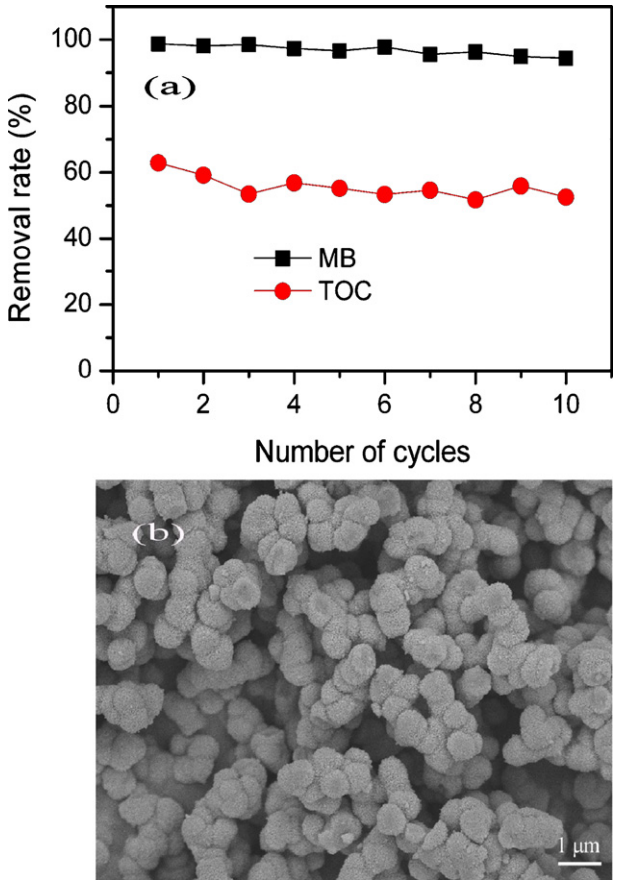

Fig. 11. (a) MB and TOC removals in the photodegradation using the same TiO_2 submicrospheres in a cycled mode, and (b) FESEM image of the reused TiO_2 submicrospheres.

MB and TOC after 10 cycles. The reused TiO_2 submicrosphere sample after 10 cycles was examined by SEM, and the image is shown in Fig. 11b. It can be seen that no cracks or broken sphere were found notably although some nanothorns were absent from the spheres. Overall, it can be seen that TiO_2 submicrospheres had good mechanical strength.

4. Conclusion

Anatase TiO_2 submicrospheres with nanothornlike rough shell were successfully fabricated at room temperature via a chemical solution deposition technique using TiF_4. Systematical investigation showed that the size, structure of the TiO_2 spheres depend on pH of the TiF_4 solution and the reaction temperature. At low pH the TiO_2 submicrospheres were compact while at higher pH and the TiO_2 submicrospheres become loose. The nanothornlike shell disappeared when increasing the reaction temperature to 60 °C. The TiO_2 submicrospheres exhibited good performance on photocatalytic oxidation of methylene blue (MB) due to the unique rough shell resulting in higher absorbance because the light can have multiple reflections among nanothorns. Membrane filtration can completely separate these TiO_2 submicrospheres form treated water without serious membrane fouling due to their large size. The durability test showed that the mechanical strength and photocatalytic activity are stable enough for multiple recycling.

References

[1] M.R. Hoffmann, S.T. Martin, W. Choi, D.W. Bahnemann, Chem. Rev. 95 (1995) 69–96.
[2] J.C. Yu, W. Ho, J. Yu, H. Yip, P.K. Wong, J. Zhao, Environ. Sci. Technol. 39 (2005) 1175–1179.
[3] A. Fujishima, T.N. Rao, D.A. Tryk, J. Photochem. Photobiol. C 1 (2000) 1–21.
[4] G. Balasubramanian, D.D. Dionysiou, M.T. Suidan, I. Baudin, J.-M. Lane, Appl. Catal. B 47 (2004) 73–84.
[5] A. Rachel, M. Subrahmanyam, P. Boule, Appl. Catal. B 37 (2002) 301–308.
[6] X.Z. Li, H. Liu, L.F. Cheng, H.J. Tong, Environ. Sci. Technol. 37 (2003) 3989–3994.
[7] S.A. Lee, K.H. Choo, C.H. Lee, H.I. Lee, T. Hyeon, W. Choi, H.H. Kwon, Ind. Eng. Chem. Res. 40 (2001) 1712–1719.
[8] R. Molinari, M. Borgese, E. Drioli, L. Palmisano, M. Schiavello, Catal. Today 75 (2002) 77–85.
[9] S. Nagaoka, Y. Hamasaki, S.-i. Ishihara, M. Nagata, K. Iio, C. Nagasawa, H. Ihara, J. Mol. Catal. A: Chem. 177 (2002) 255–263.
[10] B. Zhang, B. Chen, K. Shi, S. He, X. Liu, Z. Du, K. Yang, Appl. Catal. B 40 (2003) 253–258.
[11] X. Zhang, Y. Wang, G. Li, J. Mol. Catal. A: Chem. 237 (2005) 199–205.
[12] X. Zhang, G. Li, Y. Wang, Dyes Pigments 74 (2007) 536–544.
[13] G.K. Mor, O.K. Varghese, M. Paulose, K. Shankar, C.A. Grimes, Sol. Energy Mater. Sol. Cells 90 (2006) 2011–2075.
[14] X. Wang, J.C. Yu, C. Ho, Y. Hou, X. Fu, Langmuir 21 (2005) 2552–2559.
[15] F. Iskandar, A.B.D. Nandiyanto, K. Myoung Yun, C.J.H. Hogan Jr., K.O.P. Biswas, Adv. Mater. 19 (2007) 1408–1412.
[16] Y. Wang, H. Xu, X. Wang, X. Zhang, H. Jia, L. Zhang, J. Qiu, J. Phys. Chem. B 110 (2006) 13835–13840.
[17] H. Li, Z. Bian, J. Zhu, D. Zhang, G. Li, Y. Huo, H. Li, Y. Lu, J. Am. Chem. Soc. 129 (2007) 8406–8407.
[18] W. Ho, J.C. Yu, S. Lee, Chem. Commun. (2006) 1115–1117.
[19] Z. Liu, D. Sun, P. Guo, J. Leckie, Chem. Eur. J. 13 (2007) 1851–1855.
[20] X. Zhang, J.H. Pan, A.J.H. Du, P.F. Lee, D.D. Sun, J.O. Leckie, Chem. Lett. 37 (2008) 424–425.
[21] W.T. Yao, S.H. Yu, S.J. Liu, J.P. Chen, X.M. Liu, F.Q. Li, J. Phys. Chem. B 110 (2006) 11704–11710.
[22] Y. Gao, M. Nagai, W.-S. Seo, K. Koumoto, J. Am. Ceram. Soc. 90 (2007) 831–837.
[23] H.G. Yang, H.C. Zeng, J. Phys. Chem. B 107 (2003) 12244–12255.
[24] H. Imai, Y. Takei, K. Shimizu, M. Matsuda, H. Hirashima, J. Mater. Chem. 9 (1999) 2971–2972.
[25] S.C. Lee, H.G. Yu, J.G. Yu, C.H. Ao, J. Cryst. Growth 295 (2006) 60–68.
[26] P. Yang, M. Yang, S.L. Zou, J.Y. Xie, W.T. Yang, J. Am. Chem. Soc. 129 (2007) 1541–1552.
[27] J. Yu, W. Liu, H. Yu, Cryst. Growth Des. 8 (2008) 930–934.
[28] C.-C. Ho, A.L. Zydney, J. Colloid Interf. Sci. 232 (2000) 389–399.
[29] J.-S. Kim, C.-H. Lee, I.-S. Chang, Water Res. 35 (2001) 2137–2144.
[30] X. Zhang, J.H. Pan, A.J. Du, W. Fu, D.D. Sun, J.O. Leckie, Water Res. 43 (2009) 1179–1186.
[31] H. Imai, M. Matsuta, K. Shimizu, H. Hirashimaa, N. Negishi, J. Mater. Chem. 10 (2000) 2005–2006.
[32] X. Zhang, A.J. Du, P. Lee, D.D. Sun, J.O. Leckie, Appl. Catal. B: Environ. 84 (2008) 262–267.
[33] Z. Ding, G.Q. Lu, P.F. Greenfield, J. Phys. Chem. B 104 (2000) 4815–4820.
[34] X. Zhang, A.J. Du, P. Lee, D.D. Sun, J.O. Leckie, J. Membr. Sci. 313 (2008) 44–51.
[35] A. Sclafani, J.M. Herrmann, J. Phys. Chem. 100 (1996) 13655–13661.
[36] A. Mills, S. Le Hunte, J. Photochem. Photobiol. A 108 (1997) 1–35.
[37] X. Zhang, J.H. Pan, A.J. Du, J. Ng, D.D. Sun, J.O. Leckie, Mater. Res. Bull. 44 (2009) 1070–1076.